Chem Soc Rev

Laboratory spectroscopy of astrophysically relevant carbon species

Journal:	*Chemical Society Reviews*
Manuscript ID:	CS-REV-01-2014-000049.R1
Article Type:	Review Article
Date Submitted by the Author:	17-Mar-2014
Complete List of Authors:	Zack, Lindsay; Wayne State University, Chemistry Maier, John P; University of Basel, Chemistry

Laboratory spectroscopy of astrophysically relevant carbon species

Lindsay N. Zack[a‡] and John P. Maier*[a]

[a] Department of Chemistry, University of Basel, Klingelbergstrasse 80, CH-4056 Basel, Switzerland. Fax: +41 61 267 3855; Tel: +41 61 267 3826; E-mail: j.p.maier@unibas.ch

‡ Present Address: Department of Chemistry, Wayne State University, 5101 Cass Ave, Detroit, MI 48202, USA

submitted to Chem. Soc. Rev.: 28 January 2014
revision: 17 March 2014
16 page(s), 1 table(s), 16 figure(s)

Abstract

Carbon is one of the most common elements in the solar system, with a fractional abundance of 10^{-4} relative to hydrogen. Thus, it is not surprising that over 100 carbon-bearing species have been definitively detected in the interstellar medium via their rotational, infrared, and/or electronic transitions. In order to identify these species, laboratory spectra are needed for comparison to astronomical data. Challenges arise when obtaining laboratory spectra due to the instability of many of these molecules. Over the years, sensitive instrumentation and better techniques for producing these species in situ have been developed to achieve this goal. The use of complementary spectroscopic methods, such as matrix isolation, cavity ringdown, resonance enhanced multiphoton ionization, and ion trapping have led to the identification of several new carbon species at optical and ultraviolet wavelengths. Laboratory spectra have been compared to astronomical data in order to gain further insight into interstellar chemistry. In particular, attempts have been made to identify the carriers of the diffuse interstellar bands, however, with little success. These results are discussed in the following review.

1 Introduction

The measurement of gas-phase spectra of transient species (ions and radicals) is not a trivial task. These types of molecules are often short-lived and chemically reactive. In order to produce a sufficient quantity for analysis, exotic synthesis methods, such as laser vaporization or discharge techniques, are employed. Sensitive detection methods are then needed to obtain the spectra of these molecules, requiring complex laboratory setups. Moreover, searching for hitherto unknown molecules can be a time-consuming and arduous undertaking, therefore some advance spectroscopic knowledge, such as the approximate location of electronic transitions or spectroscopic parameters, is generally desirable. In the absence of previous experimental work, this information can sometimes be obtained from high-level theoretical calculations, which may have large amounts of error. To this end, laboratory techniques have been developed over the last 40 years to synthesize such species in situ, and measure their electronic spectra.

One class of molecules of interest in this respect are carbon-bearing species, which are ubiquitous in the interstellar medium (ISM). To date, over 150 distinct molecules have been detected in a wide range of astrophysical environments,[1–3] including circumstellar envelopes, comets, and diffuse and molecular clouds. Although the bulk of these molecules were detected at mm/sub-mm wavelengths via their pure rotational transitions, the lack of permanent dipole moments in many carbon chains and rings, as well as their derivatives and ions, make their spectra inaccessible to microwave spectroscopy and radio astronomy. Thus, infrared and electronic spectroscopy are valuable and necessary tools for characterizing the molecular content of the ISM. Carbon species, such as chains and rings, have also been proposed as the carriers of the diffuse interstellar bands (DIBs), a long-standing spectroscopic enigma.[4,5]

Laboratory techniques for measuring electronic spectra include both condensed- and gas-phase approaches. Matrix isolation methods can be used to probe a broad spectral range to initially locate regions with electronic transitions for the molecule of interest. With that information, gas-phase techniques, including cavity ringdown (CRD), degenerate four-wave mixing (DFWM), resonance-enhanced multiphoton ionization (REMPI), and ion trapping, can determine the exact positions of absorption bands for comparison to astrophysical data.[6] These methods also yield information on the geometric and electronic structure of molecules,[7] which is applicable in many other fields, such as in situ monitoring of flames, soot formation, and intermediates in chemical reactions in general.

This review describes several of the techniques currently employed for measuring the gas-phase electronic spectra of astrophysically relevant carbon species. Different interstellar environments are discussed in terms of their carbon content and in relation to electronic spectroscopy. Finally, the diffuse interstellar bands (DIBs) are considered, with a comparison of laboratory spectra to astronomical data for several carbon-containing molecules.

2 Laboratory techniques

Several laboratory techniques have been developed to produce transient carbon species in the gas phase and measure the resulting spectra. These types of molecules can be synthesized by several methods, including production in electrical discharges or with laser ablation. The molecules can then be probed by a variety of gas-phase techniques.

2.1 Synthesis of unstable molecules

Electrical discharges, which are often employed in physical and analytical chemistry, are one method of effectively producing transient molecules in the gas phase. A potential difference is applied between two electrodes in a low-pressure environment in the presence of a rare gas that may or may not be seeded with another species. A plasma is created between the electrodes and interacts with the electric field. Collisions involving electrons or cations within the plasma or on surfaces (i.e. sputtering) can result in the formation of new species through atomization or ionization mechanisms; excitation to higher electronic states can also occur.[8] The plasma can be characterized by coupling the source to a mass spectrometer, if desired.

Another method that can be used for generating transient species is laser ablation. This technique has proven effective for vaporizing several types of solid materials, including pure metal rods, alloys, and pressed powders, as well as liquid samples. The laser will evaporate or sublime the material, and convert it into a plasma. In one of the most common setups, laser ablation is used in conjunction with a supersonic jet. The ablation laser pulse is timed such that the gas from the nozzle will entrain the metal vapor. A "growth channel" may be placed after the vaporization point to encourage collisions and condensation,

which could enhance production of larger species. The gas is then expanded into the vacuum chamber where it can be probed by a variety of spectroscopic methods.[9]

2.2 Matrix isolation

One of the difficulties in measuring the laboratory electronic spectra of new molecules is the uncertainty in knowing where the transitions are located. Although ab initio and DFT methods can predict the energies of molecular electronic transitions, these calculations can have many sources of error associated with them, especially for larger radicals and ions. Thus, it is useful to have available a laboratory experiment where a specific species can be selectively probed over a broad wavelength range. Although matrix isolation is not a gas-phase technique, it is often the first step in determining the spectra of previously unknown species.

Matrix isolation can be used to record the spectra of both neutral and ionic molecules. Species of interest can be mass-selected before being deposited on a 6 K neon matrix and interrogated. Briefly, ions are produced in an electron impact, cesium sputter, or hot-cathode source and directed through a series of electrostatic lenses into a magnetic bender before being mass selected in a quadrupole mass spectrometer. They are then co-deposited with excess neon to a thickness of 100–200 μm onto a rhodium-coated sapphire plate cooled to 6 K (Fig. 1). A waveguide technique is used to focus broadband light through the matrix (effective path length ≈2 cm); exiting light is focused onto an optical bundle and detected with a CCD camera.[10]

<insert Figure 1>

This technique is particularly useful for measuring reactive species and intermediates, such as radicals and ions, which can be stabilized in a rare gas matrix.[11,12] It has also been helpful in identifying the spectra of weakly-bound molecules having hydrogen bonds or van der Waal interactions.[13] However, this method is not without certain drawbacks, as well. Because the species of interest are frozen in a rare gas lattice, rotational structure is absent and the molecules can sometimes interact with the matrix itself. Absorption features are often broadened due to site effects or phonon resonances. Moreover, there is a shift in band positions relative to the gas phase. This offset is large enough that matrix spectra cannot be used for direct comparison to astronomical data, but small enough to guide gas-phase measurements.

Recently, absorption and fluorescence spectra of protonated polycyclic aromatic hydrocarbons (H-PAH$^+$s) have been measured in 6 K neon matrices using a hot-cathode discharge source.[14,15] These molecules can be synthesized by two methods: ionization of a dihydro-PAH precursor or through proton transfer. In the former, for example, 9,10-dihydro-anthracene was used to produce protonated anthracene by stripping an H from a CH_2 group.[14] This method, however, leads to a more complicated spectrum from contamination due to fragmentation and isomerization in the matrix. A "softer" technique, proton transfer, was used to generate protonated pyrene and coronene (H-Py$^+$ and H-Cor$^+$, respectively) by reacting PAH vapor with protonated ethanol.[16] This method results in less fragmentation and it is also useful when a dihydro-PAH precursor is not available.

Protonated PAHs usually have multiple non-equivalent protonation sites. In the case of H-Py$^+$, these sites are located at carbons 1, 2, and 4. The lowest energy isomer is 1H-Py$^+$, and the absorption at 487.5 nm was assigned as the origin band of the $(1)^1A' \leftarrow X\ ^1A'$ electronic transition; other absorptions attributed to this molecule extend into the UV. The $(4)^2A' \leftarrow X\ ^2A'$ origin band of neutral H-pyrene at 389.1 nm was also observed in these experiments.

The electronic spectra of PAHs have been the focus of several astronomical observations. Anthracene and phenanthrene have been detected in Comet P/Halley via UV transitions, and pyrene has also been tentatively identified.[17–19] H-PAH$^+$s have been proposed as the carriers of the DIBs;[20] however, comparison of a recently-measured gas-phase H-Py$^+$ electronic spectrum to astronomical data has yielded a negative result (see Section 2.6).[21] Investigations of additional H-PAH$^+$ species by infrared spectroscopic techniques have not led to any matches with the unidentified infrared (UIR) emission bands.[22,23]

2.3 Cavity ringdown spectroscopy

Cavity ringdown spectroscopy (CRDS) is a sensitive direct-absorption technique that has been used in a variety of applications at infrared and optical wavelengths.[24] A sample is placed in a high-finesse optical cavity of length L formed by two highly-reflective mirrors (R > 99.9%). Laser light is coupled into the cavity, where it is reflected back and forth between the two mirrors. On each pass, a fraction of the light

leaks out, such that the signal takes the form of an exponential decay. The multiple passes translate into a much longer path length (several kilometers in some cases), and the absorption spectrum is generated by measuring the ringdown time as a function of wavelength. This method can be used with either pulsed or continuous wave lasers. A schematic of the CRDS setup is shown in Fig. 2.

<insert Figure 2>

2.3.1 Three-level depletion

One disadvantage of the CRD technique occurs in the event of optical saturation, which results in non-linear absorption signals. These effects are generally present when the pumping frequency of the laser is much faster than either the population's relaxation rate or the ringdown decay time. This disparity causes depletion in the lower energy level of the system, so the absorber cannot be described in terms of a single exponential fit. Because absorption coefficients, and thus densities of the absorbing species, are determined from fitting the decay curve, saturation effects can lead to gross underestimates of these values.[25] However, some models have been developed that decouple variations in the decay rate from background, increasing sensitivity.[26] But these methods had only been evaluated for two-level systems.

Recently, proof of this concept has been demonstrated for three-level systems, as well.[27] Two lasers, a pump, λ_2, and a probe, λ_3, are introduced into a cavity where they simultaneously excite two resonant states sharing a common level. If the decay rate of λ_3, for example, is monitored, a decrease will be noticeable in a shared lower level due to the depletion of the lower state population upon introduction of λ_2. This effect can also be measured by monitoring a population increase in a shared upper level; Fig. 3 shows the different schemes. One can determine the expected changes in ringdown times by numerically solving a series of coupled differential equations that describe a closed three-level system, which take into account level populations, power density, and Einstein coefficients. A detailed discussion is presented in Ref. 27. Experimentally, depletion in the common level can be observed by monitoring the baseline for a drop in signal when a resonant transition is scanned by the pump laser. This variant of the pulsed CRD technique has been demonstrated for atomic neon transitions, as well as some resonant rovibrational lines of the $d\ ^3\Pi_g \leftarrow a\ ^3\Pi_u$ transition of C_2.

<insert Figure 3>

2.4 Four-wave mixing

Degenerate four-wave mixing (DFWM) is a nonlinear, background free technique that offers high sensitivity (S/N ratio up to 10^4) and a large dynamic range. Moreover, its variants can be used for resonant spectroscopy giving unambiguous assignments of molecules, even in regions of spectral overlap. This method is based on the third order susceptibility tensor, which couples three input beams to some medium, generating a fourth beam. Two of the input beams are considered to be "pump" beams that form a Bragg grating through interference with the third beam, the "probe." The fourth beam is produced when a resonance occurs. Two common beam geometries are shown in Fig. 4: a) phase-conjugate and b) forward configuration. In the former, the probe beam interacts with the coaxial, counterpropagating pump beams producing a grating. The backward pump beam scatters off the grating produced from the interference between the forward pump and probe, generating a signal beam, which is the phase conjugate of the probe. In the gas phase, this is generally the most important interaction, as the fringe pattern produced from interference between the backward pump and probe is "washed out" by thermal motion.[28] In the forward geometry, comparable to the BOXCARS configuration, all of the input beams are oriented in the same direction and intersect at a single point. Two of the beams will form a grating, diffracting the third beam and generating the signal. This arrangement results in automatic phase matching and is more sensitive because all photons can be detected, in contrast to the phase-conjugate layout.[29,30]

<insert Figure 4>

Four-wave mixing techniques have been used to record the spectra of several carbon chain molecules, including C_2, C_4H, and some $HC_{2n}S$ species (n = 1, 2).[30,31] The HC_nS chains were produced in a slit-jet discharge using CS_2/HCCH gas mixtures as a precursor. The $A\ ^2\Pi_{3/2} \leftarrow X\ ^2\Pi_{3/2}$ electronic transition was measured by DWFM and resonant two-color four-wave mixing techniques (TC-RFWM) in the BOXCARS geometry. With this method, detection limits of around 10^9–10^{10} molecules cm^{-3} and S/N ratios on the order of 10^3–10^4 were obtained.

The selectivity of DFWM over CRDS is illustrated in Fig. 5. The 5_0^3 band of the C_4H $B\ ^2\Pi_i \longleftarrow X\ ^2\Sigma^+$ electronic transition lies near a hot band of the $A\ ^1\Pi_u \longleftarrow X\ ^1\Sigma_g^+$ electronic transition of C_3. With CRDS methods (top trace), it is difficult to distinguish the two molecules. However, when DFWM is used (bottom two traces), clear spectra can be obtained for both species. A striking difference is also observed between variants of four-wave mixing. Take for example, the $4_0^1 5_0^1$ band of the $A\ ^2\Pi_{3/2} \longleftarrow X\ ^2\Pi_{3/2}$ electronic transition of HC_2S, which overlaps the C_3 $A\ ^1\Pi_u \longleftarrow X\ ^1\Sigma_g^+$ origin band. When DFWM is used, contamination from C_3 makes it impossible to resolve the HC_2S spectrum, but with TC-RFWM, the HC_2S transitions are clearly separable.[31]

<insert Figure 5>

2.5 Resonance enhanced multiphoton ionization

Resonance-enhanced multiphoton ionization (REMPI) is a mass-selective, gas-phase technique used to detect neutral species via a two-step process.[32] Molecules are produced by discharge or laser ablation methods. The molecular beam is collimated through a skimmer into the interaction region of a time-of-flight mass spectrometer (TOF-MS). Here, neutrals are excited to a higher electronic state with one photon and then ionized with a second, which may or may not have the same energy (i.e. one or two color, respectively). The ions are separated in the TOF-MS, where different mass channels can be observed simultaneously, an advantageous feature for survey scans. Thus, the spectra are not measured directly; rather, the ion signal is monitored as the wavelengths are scanned. Absorptions are only detected when the species of interest is excited to a resonant state, otherwise, the second photon will not provide sufficient energy to ionize the molecule. Variations of this technique involve multiple photons for each step. The REMPI setup is shown in Fig. 6.

<insert Figure 6>

One class of molecules that has been investigated by this technique is the metal-terminated carbon chains. Significant quantities of atomic metals have been observed toward the C-rich star IRC+10216[33] and several metal-bearing species, such as MgCN, MgNC, and AlNC, to name a few, have already been detected.[34] It has been proposed that species such as AlCCH and MgCCH, for example, could form through ligand-switching or radiative association mechanisms,[35] especially given the presence of acetylenic species in circumstellar environments.[34] This proposal established the need for gas-phase spectra of this type of molecule.

Thus, resonant two-color, two-photon ionization (R2C2PI) has been used to measure the spectra of the $C\ ^2B_2 \longleftarrow X\ ^2A_1$ and $D\ ^2B_1 \longleftarrow X\ ^2A_1$ electronic transitions of the T-shaped AlC_2, the $A\ ^1\Pi \longleftarrow X\ ^1\Sigma^+$ transition of AlCCH, and the $A\ ^2\Pi \longleftarrow X\ ^2\Sigma^+$ transitions for linear $MgC_{2n}H$ (n=1–3). These transitions absorb in the visible, but oscillator strengths are calculated to decrease for the $MgC_{2n}H$ species with increasing chain length,[36] making them unlikely candidates for interstellar absorption features at visible wavelengths.

2.6 Ion trapping

The previously mentioned techniques can produce molecules with residual vibrational excitation. However, the ISM is a relatively cold environment, with temperatures often below 100 K. Thus, in order to better mimic astrophysical conditions in a terrestrial environment, ion trapping methods have been developed, where a charged molecular species is cooled through collisions with a cryogenic buffer gas. Cations are produced in an electron impact or chemical ionization source and mass selected by a quadrupole before being introduced into a 22-pole radiofrequency trap.[37] Cold helium (≈6–10 K) is flowed into the trap, where it undergoes collisions with the stored ions, equilibrating their rotational and vibrational degrees of freedom. Generally, thousands of ions are trapped per duty cycle and cooled for around 70 ms. Spectra are generated using either a one- or two-color, two-photon fragmentation technique.[38,39] The cold ions are excited with a tunable laser and then fragmented by a second laser pulse held at a fixed wavelength. The fragments are filtered out of the trap by a second quadrupole and counted while the first laser scans the electronic transition. The setup for this experiment is shown in Fig. 7.

<insert Figure 7>

Ion trapping methods have been used to record the spectra of several polyacetylene cations and nitrogen-capped carbon chain cations.[40,41] In many cases, only electronic transitions to the lowest excited electronic state are considered for comparison to DIB spectra. However, one study investigated the relevance of higher excited electronic states of polyacetylene cations ($HC_{2n}H^+$, n = 4–6).[42] Although transitions to the *B*, *C*, and *D* electronic states for these molecules fall within the DIB range and are expected to have reasonable oscillator strengths, they were traditionally excluded from consideration, as they were expected to be lifetime broadened. Measurements at 20 K, however, show that some of these species possess excited state lifetimes on the order of picoseconds, corresponding to linewidths of 1–10 cm^{-1}, or narrow enough to be potential DIBs. Although none of these cations have been associated with any DIB absorptions, this result shows that electronic transitions to higher excited states should not be neglected when investigating potential DIB carriers.

The spectra of H-Py^+ and H-Cor^+ have also been measured using a two photon photofragmentation method.[21,43] The origin band, 0_0^0, of the $(1)^1A' \leftarrow X\ ^1A'$ electronic transition of H-Py^+ lies at 4858.86 Å, blueshifted by about 2 Å relative to neon matrix data. Fig. 8 shows this transition of H-Py^+ acquired after being cooled for different lengths of time. In the bottom trace, the ions were trapped for 20 ms, corresponding to a temperature of 100 K, as evidenced by the presence of hot bands at approximately ±60 cm^{-1} to the red and blue of the 0_0^0 band. If the ions are cooled for 80 ms, however, a temperature of 15 K is reached; thus, the ions are in their vibrational ground state and the hot bands disappear (top trace). Comparison of these gas-phase H-Py^+ absorptions to astronomical data has yielded negative results. A strong Hβ line in the DIB region contaminates the location of the 0_0^0 band. No prominent DIBs correspond to other bands in the H-Py^+ spectrum.

<insert Figure 8>

2.6.1 Laser induced inhibition of complex growth

A new detection method for measuring the absorption of ions has recently been developed— laser induced inhibition of complex growth (LIICG), which does not rely on photofragmentation.[44] In this scheme, ions are irradiated in a radiofrequency trap as they are cooled, exciting the majority to a resonant state. Roughly 4–5% of the parent ions in the ground state form complexes with the buffer gas; a depletion in these complexes is observed upon laser irradiation. Fig. 9 illustrates this process for the N_2^+ system in helium. Here, N_2^+ ions in the ground electronic and vibrational states, $X\ ^2\Sigma_g^+$, v = 0, will be excited to the $A\ ^2\Pi_u$ state (rate coefficient k_{ex}), where they radiate (k_{rad}) to excited vibrational levels of the ground electronic state (N_2^+*). The competing process is the ternary association reaction (k_3) leading to formation of the N_2^+—He complex. The number of complexes is also limited by collision-induced dissociation (k_{CID}). Thus, a stationary equilibrium is present in the trap and the spectrum is measured by monitoring the number of complexes. Although this technique has only been tested with the N_2^+—He system,[44] it can be applied to other polyatomic cations, including carbon-containing systems.

<insert Figure 9>

Fig. 10 shows the LIICG electronic spectrum of the $A\ ^2\Pi_u \leftarrow X\ ^2\Sigma_g^+$ (2, 0) transition of N_2^+, with the number of N_2^+—He complexes plotted as a function of wavelength. A decrease in the number of complexes is observed when the laser scans over a resonant transition of N_2^+. Rotational structure is well-resolved for most of the absorptions, with splittings due to electronic fine structure and nuclear spin statistics clearly present. It is important to note that the spectrum results from absorptions of the bare N_2^+ ion.

<insert Figure 10>

3 The interstellar medium

The ISM consists of several unique and distinct environments spanning a large range of densities and temperatures. The physical conditions of these regions directly affect the chemistry and are reflected in the types of molecules present.[45] A wealth of spectroscopic data toward comets, circumstellar envelopes, and diffuse and molecular clouds has been collected. Molecular detections include small radicals and ions, metal- and silicon-bearing species, carbon chains, and complex organics.[2,3] Among other carbonaceous species likely present in the ISM are nanotubes, soot, and fullerene structures.[46] Carbonaceous species in

these extreme environments have generated quite a bit of interest due to their possible astrobiological connection.[46,47] Physical properties of different regions are listed in Table 1.

<insert Table 1>

3.1 Comets

Comets are one of the most variable chemical laboratories in the ISM. The majority of comets originate in the Oort cloud or Kuiper Belt, so they are often considered to be sources of "pristine" material reflective of the composition of the protosolar nebula. Most comets consist of four main components— a nucleus, a coma, an ionic tail, and a dust tail, each having different characteristics. The nucleus is often described as a "dirty snowball," reflecting its rough composition of dust and ice. As the comet approaches the sun, the nucleus outgasses and molecules sublimate forming a dusty atmosphere, or coma. Here, one can observe the fluorescence of the species evaporated from the nucleus ("parents"), as well as the photodissociated radical and/or ionic "daughter" species. The two types of tails result from the interaction of the coma with the solar wind (ion tail) and radiation pressure (dust tail). Physical conditions in comets can be quite variable depending on the distance from the sun and other factors, with densities and temperatures ranging from $10–10^{12}$ cm^{-3} and 10–100 K, respectively.[48] There can also be large variations from comet to comet.

The earliest cometary spectra were taken in 1864 on photographic plates[49] and identified four years later as belonging to the C_2 Swan bands by comparison with flame spectra.[50] These bands have subsequently been detected in every comet. Although the main component of comets is water, several carbon-containing species have been observed.[2] In fact, CN or C_2 often dominate the optical spectra, and at larger distances from the sun, the 4050 Å band of C_3 increases in intensity relative to other species.[51] In most cometary spectra, tens of thousands of lines are usually reported, thousands of which often remain unidentified.[52,53] These lines could possibly be due to carbon species.

3.2 Circumstellar envelopes and evolved stars

Elemental carbon is produced in the cores of intermediate mass stars through the triple alpha process and the CNO cycle when the star is on the red giant or asymptotic giant branch (AGB). Dredge-up events bring the carbon to the surface, where it can form gas-phase molecules or condense into/onto grains and ices. After the AGB, the star evolves into a protoplanetary nebula (PPN) and will finally become a planetary nebula (PN), where its circumstellar envelope (CSE) is completely detached.[54] Not surprisingly, a multitude of carbon species have been observed across this evolution, including long carbon chains up to nine atoms (C_8H) at millimeter and infrared wavelengths.[55,56] Smaller carbon species, such as C_2, CN, and CH^+, have also been identified in the optical spectra of post-AGB circumstellar envelopes.[57] Additionally, detections of C_{60} and C_{70} via IR emission in PNe have been reported.[58,59] Molecules from these sources, if not destroyed by cosmic radiation, can seed other environments, contributing to the recycling of interstellar material.

3.3 Clouds

Interstellar clouds can be classified into three main types: diffuse, translucent, and dense, which vary in terms of typical temperature and number density (Table 1). The physical conditions of these environments is reflective of their molecular composition. Although these distinctions exist in a general sense, it is important to note that clouds are neither uniform nor quiescent, and that even vastly different environments can be homes to the same or similar types of molecules. The composition, especially in dense media, is generally clumpy and may have a gradient of temperatures and densities. For example, a molecular cloud is often surrounded by a diffuse, photon-dominated region and may have very dense cores embedded throughout.[60]

Diffuse clouds are often rich in both atomic and small molecular species. The cosmic radiation field can easily penetrate the low-density media, dissociating and ionizing the remnant material from CSEs and PNe present in this environment. Thus, diffuse clouds are generally characterized by the presence of radicals and/or ions. The low density environment makes millimeter-wave astronomical observations difficult, so these often have to be conducted in absorption against a background star. In this way, several molecules such as HCO^+ (J = 1-0), C_2H (N = 0-1), HCN (N = 0-1) have been detected.[61] Optical observations of diffuse interstellar media have also been performed towards several lines of sight, identifying a similar set of molecules. The most distinctive features from the optical observations are the diffuse interstellar bands (DIBs), which are discussed in Section 4.

Dense, or molecular, clouds are characterized by the presence of long carbon-chain molecules, such as cyanopolyynes, cumulenic carbenes, and methylated carbon chains and complex organic molecules, including methyl acetate, ethanimine, and glycoaldehyde.[1] Many of these species are considered to be astrobiologically relevant and are thought to form on the surfaces of grains.[1] Complicated reaction networks are often constructed to describe possible formation mechanisms. Observations of these sources are almost exclusively through mm-wave astronomy. However, infrared absorption astronomy has also been used to identify C_2H_2,[62] CO,[63] and CH_4,[64] among others.

4 Comparison of laboratory spectra to diffuse interstellar bands

Perhaps one of the most intriguing mysteries in observational astronomy is the identity of the diffuse interstellar band (DIB) carriers. The DIBs comprise over 500 absorption features in the 4400–9000 Å range.[5,65] Initially, it was assumed that these features were due to dust grains or pre-dissociated molecules, however both of these explanations have since been ruled out. It has been proposed that carbon chains are responsible for the DIBs,[4] thus much effort has been expended to explore this suggestion. In addition to pure carbon chains and rings, several species that include hydrogen, nitrogen, and/or sulfur atoms attached to a carbon backbone have also been investigated.

Although several laboratory techniques are available for the measurement of such types of molecules, not every method is appropriate for a specific molecule, so the advantages and disadvantages of each technique must be evaluated. The spectra of ionic species, for example, can be recorded using CRDS, DFWM and its variants, and ion trapping methods. However, CRDS and DFWM are more suitable for achieving rotational resolution, whereas ion trapping can be used when it is necessary to obtain cold spectra. For neutrals, REMPI, CRDS, or DFWM work well, but REMPI dictates certain restrictions regarding a molecule's ionization energy, which are absent for CRDS and DFWM. On the other hand, the mass-selectivity of the REMPI technique make it advantageous over CRDS or DFWM in many cases.

Generally, a direct comparison of laboratory and astronomical data is difficult. Astronomical spectra can be contaminated when several objects reside along the sightline of the cloud of interest, especially when that source is in or near the galactic plane. Broadening of spectral lines can occur due to interstellar conditions, and one must also be conscious of the temperature of the local environment. Nonetheless, observational data are often able to constrain the physical conditions quite well, making comparison between laboratory and telescope data possible once the laboratory spectra are corrected for these factors. Thus, experimental spectra of several carbon-bearing species have been compared to astronomical data of DIBs. Although several intriguing similarities are noted between the datasets, with the exception of C_3, definitive identifications have not been made of the DIB carriers. Regardless, these comparisons can still provide information about the chemical inventory and physical characteristics of astrophysical environments. Moreover, resemblances (or contrasts) between laboratory and astronomical spectra furnish clues as to the actual carriers of the DIBs, such that future searches can be directed toward specific molecular classes.

Past comparisons of laboratory and astronomical data have led to the establishment of certain criteria that must be considered when choosing appropriate target molecules. First, and almost trivially, the molecule must have electronic transitions in the DIB range. Fig. 11 shows a plot of the origin band wavelengths vs. chain length for a several odd-number carbon chains and ions. It is clear that some species that make chemical sense clearly cannot be responsible for the DIBs because they lack electronic transitions in this range. A second criterion is that, in order to contribute to stronger DIBs, the carrier must have an oscillator strength in the 1–10 range. This condition is due to upper limits to the column densities for these species being on the order of 10^{11} cm^{-2}, and the typical equivalent width of the DIBs is 0.1 Å.

<insert Figure 11>

4.1 Carbon chains: C_3, C_4, and C_5

The laboratory spectrum of the C_3 $A\ ^1\Pi_u \leftarrow X\ ^1\Sigma_g+$ origin band near 4052 Å was compared to astronomical data taken at the Canada-France-Hawaii telescope on Mauna Kea,[66] as shown in Fig. 12. Here, the electronic spectrum is simulated based on the observed line positions with intensities calculated using Hönl-London factors and assuming a rotational temperature of 80 K. The rotational profile is clearly superimposable on the astronomical spectra taken toward three stars: 20 Aql, ζ Oph, and ζ Per, marking a clear detection of C_3 in these clouds. From these data, a column density of $N(C_3) \approx 1–2\times10^{12}$ cm^{-2} can be inferred, consistent with values subsequently obtained towards several other sightlines.[67]

<insert Figure 12>

Following the successful identification of C_3 towards diffuse clouds, a search was conducted for longer carbon chains. The $^3\Sigma_u^- \longleftarrow X\ ^3\Sigma_g^-$ and $^1\Pi_u \longleftarrow X\ ^1\Sigma_g^+$ electronic transitions of C_4 and C_5, respectively, were looked for in ζ Oph, but with negative results. Upper limits to the column densities of these species were determined to be $N(C_4) \leq 5\times10^{11}$ cm^{-2} and $N(C_5) \leq 1\times10^{11}$ cm^{-2}.[68] Searches for C_4 and C_5 toward a different source, HD 204728, also yielded negative results with corresponding upper limits of $N(C_4) \leq 2\times10^{12}$ cm^{-2} and $N(C_5) \leq 5\times10^{12}$ cm^{-2}.[67] However, these values are based on theoretical, rather than experimental, oscillator strengths, which introduces uncertainty into these estimates.

From the derived column densities and upper limits of C_3, C_4, and C_5, it is possible to calculate fractional abundances of these species relative to H_2 for comparison to diffuse cloud models. Assuming $N(H_2) = 3\times10^{20}$ cm^{-2} in ζ Oph, [69] fractional abundances are 5.3×10^{-9}, 1.7×10^{-9}, and 3.3×10^{-10} for C_3, C_4, and C_5, respectively. The C_3 abundance agrees quite well with that calculated by a multi-level excitation model, 4.8×10^{-9}.[70] Estimates of fractional abundances for C_4 and C_5 toward HD 21012, a slightly denser and redder source than ζ Oph, are around 1.5×10^{-9} and 1.1×10^{-9}, respectively. Thus, while this model predicts abundances of C_3 and C_4 toward diffuse clouds quite accurately, a breakdown seems to occur with C_5. This discrepancy between the observed and calculated abundances of C_5 might indicate that the model may be missing crucial information regarding the formation and destruction mechanisms of longer carbon chains.

4.2 C_7^- and $C_3H_2^-$

Ionic species containing carbon are also potential candidates for DIB carriers, as interstellar radiation can easily penetrate diffuse clouds, resulting in a significant degree of ionization. The presence of several ionic carbonaceous species has even been confirmed toward dense clouds and circumstellar envelopes via radio astronomy.[71] Additionally, some ions satisfy the previously-mentioned criteria, as seen in Fig. 11. It has been observed that the laboratory spectra of several carbon chain anions, C_n^- (n = 6–9), seemingly correspond to weak DIBs.[72] Attempts to confirm these matches have yielded negative or inconclusive results,[73] as have searches for C_2^- and C_3^-.[68]

Some interesting similarities have been noted in comparisons of experimental and astrophysical data, however, with regard to ionic carbon species. Laboratory spectra of several vibrational bands of the $A\ ^2\Pi_u \longleftarrow X\ ^2\Pi_g$ transition of C_7^- seem to match up quite well with several DIBs in the 4900–6300 Å range both in wavelength and intensity.[73] A fourth band of C_7^- is also present in this region, and its intensity is consistent, but there is a 2 Å shift relative to the laboratory data— enough to call the identification of C_7^- as this DIB carrier into question.[73]

Another intriguing case is the anion $C_3H_2^-$, for which the $K = 1 \longleftarrow 0$ component of the $^2A_1 \longleftarrow {}^2B_1$ electronic transition was measured in the laboratory at a temperature of 50 K. A molecule with such a large dipole moment would be expected to cool to 3 K in the ISM, leading to a narrowing and redshifting of absorption profiles. Within experimental error, and taking the temperature uncertainty into account, the 0_0^0, 6_0^2, 4_0^1, and 2_0^1 vibronic bands correspond to weak, narrow DIBs.[74] However, when the profiles of these transitions are simulated with constants obtained from high-resolution laboratory data, certain discrepancies in shapes, intensity patterns among vibronic components, and central wavelengths are noted.[75] Thus, it has been concluded that $C_3H_2^-$ is not the carrier of these DIBs.

4.3 NC_4N^+

The rotational profile of the origin band of the $A\ ^2\Pi_g \longleftarrow X\ ^2\Pi_u$ transition of NC_4N^+ was predicted using experimentally-determined spectroscopic constants over the temperature range 3–150 K with clear differences seen in the band profiles, including shifts in position (Fig. 13).[76] This change illustrates the influence that even small variations in temperature can have on a molecule's spectrum and emphasizes the importance of constraining the cloud temperature. However, it is not always easy to determine the actual temperature, because the DIBs are often observed through several clouds, as shown by atomic K I and Ca I lines. Comparison of these profiles to DIBs around 5960 Å implies that the rotational temperature of these sources could be around 80 K. Although there is good agreement between the laboratory and astronomical line profiles, there is a 0.9 Å shift in wavelength— too large of a discrepancy to be accounted for by temperature differences.

<insert Figure 13>

In the case of NC_4N^+, as well as the previously mentioned C_7^- and $C_3H_2^-$, slight wavelength disparities were noted between experimental and astronomical data. It has recently been suggested that the DIB carriers could possibly originate from absorptions of atoms, molecules, or ions ("seeds") embedded in a shell of H_2 molecules.[77] Interactions between the seed and the H_2 molecules would cause shifts in line positions. Simulations of spectral profiles of such clusters with varying seed geometries have in some cases reproduced the line profiles of certain DIBs. However, experimental data are needed to confirm or invalidate this proposal.

4.4 C_{18}

An examination of the electronic spectrum of cyclic C_{18} in the gas phase also raises some interesting questions regarding the identity of the DIB carriers. The laboratory spectrum of this species was obtained at 50 K in the gas phase using the R2C2PI technique,[78] allowing direct comparison to DIB data. Spectra taken toward ζ Oph and HD 204827 near the origin band at 5928 Å did not yield any matches.[79] This is not surprising, considering the low oscillator strength ($f \approx 0.01$) expected for this electronic transition of C_{18}. However, the rotational profile of the origin band over a 20–100 K temperature range is very similar to some DIBs observed at different wavelengths (Fig. 14). This similarity in the spectra could imply that molecules with related structures are responsible for those absorptions. C_{18} is a monocyclic, fully dehydrogenated aromatic ring. It is possible, therefore, that some of the unidentified features in the astrophysical data are caused by large mono- or polycyclic ring structures composed of 50-100 carbon atoms with varying degrees of dehydrogenation and ionization. PAHs have been proposed as potential DIB carriers; perhaps there is a link in diffuse cloud chemistry between large, planar, dehydrogenated carbon rings and PAHs.

<insert Figure 14>

4.5 *l* – C_3H_2

Propadienylidene, *l*–C_3H_2, has been suggested as the carrier for the DIBs located near 5450 and 4881 Å. However, as the 4881 Å absorption is contaminated by a strong H β line at 4861 Å, most of the attention has been focused on comparison of laboratory spectra to the 5450 Å absorption. The $B\ ^1B_1 \longleftarrow X\ ^1A_1$ transition of *l*–C_3H_2 was measured using CRD techniques and bears a strong resemblance in both position and shape to the 5450 Å DIB. Under this assumption, and using an oscillator strength of $f \approx 0.0016$, a column density of 5×10^{14} cm^{-2} was calculated.[80] However, as previous mm-wave observations of *l*–C_3H_2 toward diffuse sources had placed an upper limit to the column density as 10^{11} cm^{-2},[81] three orders of magnitude lower, this assignment was questioned.[82] An additional attempt was made to confirm the detection by radio astronomy, however, the observations were consistent with the previous measurements— column density $N_{tot} \leq (1–3)\times10^{11}$ cm^{-2}.[83] From these results, one can infer that *l*–C_3H_2 is not solely responsible for the 5450 Å DIB; it may still contribute to the intensity of the absorption, but there must be another species absorbing at the same wavelength, as well.

4.6 HC_4H^+ and HC_6H^+

The $A\ ^2\Pi_g \longleftarrow X\ ^2\Pi_u$ origin band of the diacetylene cation, HC_4H^+, was proposed as the carrier of the weak 5069 Å DIB, based on a comparison of a laboratory CRD spectrum and astronomical data.[84] This suggestion is questionable for several reasons. When the rotational profile is predicted over a temperature range of 50–80 K , there are clear differences in the band shape due to changes in the populations of the spin components. Another aspect that could affect the line profile is the uncertainty caused by the spread of velocities in interstellar clouds. If the experimental data are also corrected for this factor, the laboratory spectrum bears little resemblance to the 5069 Å DIB, as Fig. 15 shows.[85]

<insert Figure 15>

In the case of a molecule with a $^2\Pi_i$ ground electronic state, rotational populations of the two spin ladders can also be affected by weak magnetic dipole transitions. Here, depopulation of the Ω = 1/2 spin

component to the Ω = 3/2 ladder in the electronic ground state, or $X\ ^2\Pi_{1/2} \longrightarrow X\ ^2\Pi_{3/2}$, results in non-Boltzmann distributions;[86] see bottom traces in Fig. 15. The rates of these transitions can be faster than the collision rates with atomic hydrogen in diffuse clouds (10^{-6} s^{-1} vs. 10^{-8} s^{-1}).[85] These types of transitions could provide a means for radio astronomers to observe non-polar molecules for the first time.

The $A\ ^2\Pi_g \longleftarrow X\ ^2\Pi_u$ transition of the triacetylene cation, HC_6H^+, near 6002 Å illustrates the spectroscopic concerns and physical conditions of diffuse clouds which must be considered when comparing laboratory and astronomical data. An experimental spectrum of the origin band of HC_6H^+ was obtained at 25 K using a two-color, two-photon excitation-dissociation method in a 22-pole ion trap (Fig. 16).[38] A collisional-radiative rate model was used to predict rotational profiles over a range of collision partner densities in order to mimic varying cloud conditions. This species has a $X\ ^2\Pi_{3/2}$ ground electronic state, thus its rotational profile will have a non-Boltzmann distribution, as described above. These factors were included when generating the rotational profiles, with resolved *J* lines, shown in the bottom four traces in Fig. 16. Overlaid on top of the rotational fits are contours produced when a velocity dispersion of 18 km s^{-1} is assumed. The top trace is a 25 K simulated spectrum.

<insert Figure 16>

5 Summary

Improvements in laboratory techniques over the past few decades have led to the measurement of electronic spectra of several transient, carbon-bearing molecules. Matrix isolation methods are initially used to locate band positions for species of interest. These electronic transitions can then be probed in the gas phase by several different approaches, including ion trapping, CRD, and/or REMPI. The variety of techniques employed ensures that many different types of molecules, such as neutrals, ions, and radicals, can be accessed. Synthesis of unstable species, while still challenging, has been simplified by improvements in methods involving electrical discharges and laser ablation. The gas-phase spectra of such molecules provide more precise transition energies, such that comparison to astronomical spectra can be made.

One goal of this work has been to study potential DIB carriers. Astronomical observations have provided data on the physical conditions in interstellar environments, including temperatures, densities, and velocity dispersions. From this information, laboratory spectra can be corrected for direct DIB comparisons. Through the success of C_3, and several disappointments, criteria have been established to evaluate claims that DIB carriers have been identified. Namely, the laboratory and DIB spectra must correspond in width, rotational profile, and central wavelength for all vibrational bands in a given electronic transition. Additionally, the species must make chemical sense, have electronic transitions in the DIB range, and have a sufficiently large oscillator strength. Previous studies also seem to point toward certain types and/or classes of molecules on which one should focus. Namely, long carbon chains (C_{17}, C_{19}, …) or ring systems comprised of more than 50 atoms, as well as metal-containing molecules are a logical extension. Given these criteria, the identity of another DIB carrier may one day be known.

Acknowledgements

The studies presented here have only been possible due to the motivation and ability of a number of Ph.D. students and postdoctoral fellows, who are authors in the cited articles. This research has been supported by the Swiss National Science Foundation (current project 200020-140316/1) and by the European Research Council (ERC-AdG-ElecSpecIons:246998).

References

1. E. Herbst and E. F. van Dishoeck, *Annu. Rev. Astron. Astrophys.*, 2009, **47**, 427–480, and references therein.
2. The Astrochymist, http://astrochymist.org, (accessed January 2014), and references therein.
3. The Cologne Database for Molecular Spectroscopy, http://www.astro.uni-koeln.de/cdms/molecules, (accessed January 2014).
4. A. E. Douglas, *Nature*, 1977, **269**, 130–132.
5. P. J. Sarre, *J. Mol. Spectrosc.*, 2006, **238**, 1–10.
6. E. B. Jochnowitz and J. P. Maier, *Annu. Rev. Phys. Chem.*, 2008, **59**, 519–44, and references therein.
7. M. D. Morse, *Chem. Rev.*, 1988, **86**, 1049–1109, and references therein.
8. A. Bogaerts and R. Gijbels, *Spectrochim. Acta Part B At. Spectrosc.*, 1998, **53**, 1–42, and references therein.
9. M. A. Duncan, *Rev. Sci. Instrum.*, 2012, **83**, 041101, and references therein.
10. A. Nagy, I. Garkusha, J. Fulara, and J. P. Maier, *Phys. Chem. Chem. Phys.*, 2013, **15**, 19091–101, and references therein.
11. M. E. Jacox, *Chem. Soc. Rev.*, 2002, **31**, 108–115, and references therein.
12. M. E. Jacox, *Int. J. Mass Spectrom.*, 2007, **267**, 268–276.
13. D. W. Ochsner, D. W. Ball, and Z. H. Kafafi, Eds., *A Bibliography of Matrix Isolation Spectroscopy: 1985-1997*, Naval Research Laboratory, Washington, D. C., 1998, and references therein.
14. I. Garkusha, J. Fulara, A. Nagy, and J. P. Maier, *Astrophys. J.*, 2011, **728**, 131.
15. I. Garkusha, J. Fulara, and J. P. Maier, *J. Mol. Struct.*, 2012, **1025**, 147–150.
16. I. Garkusha, J. Fulara, P. J. Sarre, and J. P. Maier, *J. Phys. Chem. A*, 2011, **115**, 10972–8.
17. G. Moreels, J. Clairemidi, P. Hermine, P. Brechignac, and P. Rousselot, *Astron. Astrophys.*, 1994, **282**, 643–656.
18. J. Clairemidi, G. Moreels, O. Mousis, and P. Bréchignac, *Astron. Astrophys.*, 2008, **492**, 245–250.
19. J. Clairemidi, P. Bréchignac, G. Moreels, and D. Pautet, *Planet. Space Sci.*, 2004, **52**, 761–772.
20. A. Pathak and P. J. Sarre, *Mon. Not. R. Astron. Soc.*, 2008, **391**, L10–L14.
21. F.-X. Hardy, O. Gause, C. A. Rice, and J. P. Maier, *Astrophys. J. Lett.*, 2013, **778**, L30.
22. O. Dopfer, *EAS Publ. Ser.*, 2011, **46**, 103–108.
23. H. Knorke, J. Langer, J. Oomens, and O. Dopfer, *Astrophys. J.*, 2009, **706**, L66–L70.
24. M. D. Wheeler, S. M. Newman, A. J. Orr-Ewing, and M. N. R. Ashfold, *J. Chem. Soc. Faraday Trans.*, 1998, **94**, 337–351, and references therein.
25. P. Macko, G. Cunge, and N. Sadeghi, *J. Phys. D. Appl. Phys.*, 2001, **34**, 1807–1811.
26. G. Giusfredi, S. Bartalini, S. Borri, P. Cancio, I. Galli, D. Mazzotti, and P. De Natale, *Phys. Rev. Lett.*, 2010, **104**, 110801.
27. F. J. Mazzotti, L. Barrios, R. Raghunandan, and J. P. Maier, *Mol. Phys.*, 2013, **111**, 335–344.
28. G. Hall and B. J. Whitaker, *J. Chem. Soc. Faraday Trans.*, 1994, **90**, 1–16.
29. G. Meijer and D. W. Chandler, *Chem. Phys. Lett.*, 1992, **192**, 1–4.
30. F. J. Mazzotti, E. Achkasova, R. Chauhan, M. Tulej, P. P. Radi, and J. P. Maier, *Phys. Chem. Chem. Phys.*, 2008, **10**, 136–41.
31. R. Raghunandan, F. J. Mazzotti, R. Chauhan, M. Tulej, and J. P. Maier, *J. Phys. Chem. A*, 2009, **113**, 13402–6.
32. M. N. R. Ashfold and J. D. Howe, *Annu. Rev. Phys. Chem.*, 1994, **45**, 57–82, and references therein.
33. N. Mauron and P. J. Huggins, *Astron. Astrophys.*, 2010, **513**, A31.
34. L. M. Ziurys, *Proc. Natl. Acad. Sci. U. S. A.*, 2006, **103**, 12274–9, and references therein.
35. S. Petrie, *Mon. Not. R. Astron. Soc.*, 1996, **282**, 807–819.
36. H. Ding, C. Apetrei, Ł. Chacaga, and J. P. Maier, *Astrophys. J.*, 2008, **677**, 348–352.
37. D. Gerlich and S. Horning, *Chem. Rev.*, 1992, **92**, 1509–1539, and references therein.
38. S. Chakrabarty, C. A. Rice, F. J. Mazzotti, R. Dietsche, and J. P. Maier, *J. Phys. Chem. A*, 2013, **117**, 9574–9577.
39. A. Dzhonson and J. P. Maier, *Int. J. Mass Spectrom.*, 2006, **255-256**, 139–143.
40. A. Dzhonson, E. B. Jochnowitz, and J. P. Maier, *J. Phys. Chem. A*, 2007, **111**, 1887–90.
41. C. A. Rice, V. Rudnev, S. Chakrabarty, and J. P. Maier, *J. Phys. Chem. A*, 2010, **114**, 1684–7.
42. C. A. Rice, V. Rudnev, R. Dietsche, and J. P. Maier, *Astron. J.*, 2010, **140**, 203–205.
43. C. A. Rice, F.-X. Hardy, O. Gause, and J. P. Maier, *J. Phys. Chem. Lett.*, 2014, **5**, 942–945.
44. S. Chakrabarty, M. Holz, E. K. Campbell, A. Banerjee, D. Gerlich, and J. P. Maier, *J. Phys. Chem. Lett.*, 2013, **4**, 4051–4054.
45. R. I. Kaiser, *Chem. Rev.*, 2002, **102**, 1309–58, and references therein.
46. P. Ehrenfreund and S. B. Charnley, *Annu. Rev. Astron. Astrophys.*, 2000, **38**, 427–483, and references therein.
47. P. Ehrenfreund and J. Cami, *Cold Spring Harb. Perspect. Biol.*, 2010, **2**, a002097, and references therein.

48. J. Crovisier, *Mol. Phys.*, 2006, **104**, 2737–2751, and references therein.
49. G. B. Donati, *Astron. Nachrichten*, 1864, **62**.
50. W. Huggins, *Philos. Trans. R. Soc. London*, 1868, **158**, 529–564.
51. M. C. Festou, H. Rickman, and R. M. West, *Astron. Astrophys. Rev.*, 1993, **4**, 363–447, and references therein.
52. A. L. Cochran and W. D. Cochran, *Icarus*, 2002, **157**, 297–308.
53. P. D. Feldman, *Phys. Scr.*, 2005, **T119**, 7–12.
54. B. W. Carroll and D. A. Ostlie, *An Introduction to Modern Astrophysics*, Addison-Wesley, 2nd edn., 2006, and references therein.
55. A. J. Remijan, J. M. Hollis, F. J. Lovas, M. A. Cordiner, T. J. Millar, A. J. Markwick-Kemper, and P. R. Jewell, *Astrophys. J.*, 2007, **664**, L47–L50.
56. P. F. Bernath, *Adv. Sp. Res.*, 1995, **15**, 15–23.
57. E. J. Bakker, E. F. van Dishoeck, L. B. F. M. Waters, and T. Schoenmaker, *Astron. Astrophys.*, 1997, **323**, 469–487.
58. J. Cami, J. Bernard-Salas, E. Peeters, and S. E. Malek, *Science*, 2010, **329**, 1180–2.
59. K. Sellgren, M. W. Werner, J. G. Ingalls, J. D. T. Smith, T. M. Carleton, and C. Joblin, *Astrophys. J. Lett.*, 2010, **722**, L54–L57.
60. T. P. Snow and B. J. McCall, *Annu. Rev. Astron. Astrophys.*, 2006, **44**, 367–414, and references therein.
61. H. S. Liszt, J. Pety, and R. Lucas, *Astron. Astrophys.*, 2008, **486**, 493–496.
62. J. H. Lacy, N. J. Evans II, J. M. Achtermann, D. E. Bruce, J. F. Arens, and J. S. Carr, *Astrophys. J.*, 1989, **342**, L43–L46.
63. B. T. Soifer, R. C. Puetter, R. W. Russell, S. P. Willner, P. M. Harvey, and F. C. Gillett, *Astrophys. J.*, 1979, **232**, L53–L57.
64. J. H. Lacy, J. S. Carr, N. J. Evans II, F. Baas, J. M. Achtermann, and J. F. Arens, *Astrophys. J.*, 1991, **376**, 556–560.
65. G. H. Herbig, *Annu. Rev. Astron. Astrophys.*, 1995, **33**, 19–73, and references therein.
66. J. P. Maier, N. M. Lakin, G. A. H. Walker, and D. A. Bohlender, *Astrophys. J.*, 2001, **553**, 267–273.
67. T. Oka, J. A. Thorburn, B. J. McCall, S. D. Friedman, L. M. Hobbs, P. Sonnentrucker, D. E. Welty, and D. G. York, *Astrophys. J.*, 2003, **582**, 823–829.
68. J. P. Maier, G. A. H. Walker, and D. A. Bohlender, *Astrophys. J.*, 2004, **602**, 286–290.
69. K. France, N. Nell, R. Kane, E. B. Burgh, M. Beasley, and J. C. Green, *Astrophys. J. Lett.*, 2013, **772**, L9.
70. E. Roueff, P. Felenbok, J. H. Black, and C. Gry, *Astron. Astrophys.*, 2002, **384**, 629–637.
71. M. C. McCarthy, in *American Astronomical Society Meeting Abstracts #214*, 2009.
72. M. Tulej, A. Kirkwood, M. Pachkov, and J. P. Maier, *Astrophys. J.*, 1998, **506**, L69–L73.
73. B. J. McCall, D. G. York, and T. Oka, *Astrophys. J.*, 2000, **531**, 329–335.
74. F. Güthe, M. Tulej, M. V. Pachkov, and J. P. Maier, *Astrophys. J.*, 2001, **555**, 466–471.
75. B. J. McCall, T. Oka, J. Thorburn, L. M. Hobbs, and D. G. York, *Astrophys. J.*, 2002, **567**, L145–L148.
76. T. Motylewski, H. Linnartz, O. Vaizert, J. P. Maier, G. A. Galazutdinov, F. A. Musaev, J. Krełowski, G. A. H. Walker, and D. A. Bohlender, *Astrophys. J.*, 2000, **531**, 312–320.
77. L. S. Bernstein, F. O. Clark, and D. K. Lynch, *Astrophys. J.*, 2013, **768**, 84.
78. A. E. Boguslavskiy, H. Ding, and J. P. Maier, *J. Chem. Phys.*, 2005, **123**, 34305.
79. J. P. Maier, A. E. Boguslavskiy, H. Ding, G. A. H. G. A. H. Walker, and D. A. Bohlender, *Astrophys. J.*, 2006, **640**, 369–372.
80. J. P. Maier, G. A. H. Walker, D. A. Bohlender, F. J. Mazzotti, R. Raghunandan, J. Fulara, I. Garkusha, and A. Nagy, *Astrophys. J.*, 2011, **726**, 41.
81. J. Cernicharo, P. Cox, D. Fossé, and R. Güsten, *Astron. Astrophys.*, 1999, **351**, 341–346.
82. T. Oka and B. J. McCall, *Science*, 2011, **331**, 293–4.
83. H. Liszt, P. Sonnentrucker, M. Cordiner, and M. Gerin, *Astrophys. J. Lett.*, 2012, **753**, L28.
84. J. Krełowski, Y. Beletsky, G. a. Galazutdinov, R. Kołos, M. Gronowski, and G. LoCurto, *Astrophys. J. Lett.*, 2010, **714**, L64–L67.
85. J. P. Maier, S. Chakrabarty, F. J. Mazzotti, C. A. Rice, R. Dietsche, G. A. H. Walker, and D. A. Bohlender, *Astrophys. J. Lett.*, 2011, **729**, L20.
86. M. D. Morse and J. P. Maier, *Astrophys. J.*, 2011, **732**, 103.
87. E. B. Jochnowitz and J. P. Maier, *Mol. Phys.*, 2008, **106**, 2093–2106, and references therein.
88. C. A. Rice and J. P. Maier, *J. Phys. Chem. A*, 2013, **117**, 5559–66, and references therein.
89. P. J. Sarre, J. R. Miles, T. H. Kerr, R. E. Hibbins, S. J. Fossey, and W. B. Somerville, *Mon. Not. R. Astron. Soc.*, 1995, **277**, L41–L43.

Table 1 Typical properties of interstellar environments

Environment	Density (cm^{-3})	T (K)	Representative Molecules
Cometary	$10^1 – 10^{12}$	10 – 100	C_2, C_3, HCN, H_2O
Circumstellar	variable	variable	carbon chains, metal-bearing species
Cloud:			
Diffuse	$10^1 – 10^2$	100	HCO^+, C_2H, CH^+
Translucent	$10^2 – 10^3$	50	C_2, C_3, OH, HCN, CH^+
Dense	$10^3 – 10^6$	10	long carbon chains, complex organics

Figure Captions:

Figure 1: Setup for the matrix isolation experiment. The inset shows a close-up view illustrating the waveguide technique. Reproduced from Ref. 10 with permission from the PCCP Owner Societies.

Figure 2: Block diagram of a cavity ringdown experiment. Tunable visible radiation is produced by a dye laser before being directed through a series of optics and into a vacuum chamber capped by two high-reflectivity mirrors. The electronics shown control the timing sequence for the lasers, gas pulse/discharge, and data acquisition.

Figure 3: Three-level system for the depletion experiments, where the lower, upper, or middle level is shared. The blue arrows represent the pump laser (λ_2), and the red arrows portray the probe laser (λ_3).

Figure 4: Different configurations of a four-wave mixing setup: a) phase-conjugate and b) forward BOXCARS.

Figure 5: The selectivity of the four-wave mixing method by comparison of spectra obtained with both CRDS and DFWM. The $B\,^2\Pi_i \leftarrow X\,^2\Sigma^+$ electronic transition of C_4H is contaminated by a C_3 hot band in the CRDS spectrum (top trace). Altering the timing of the discharge pulse while using DFWM leads to a clear separation of the two species. Reprinted from Ref. 31 with permission from the Journal of Physical Chemistry A. Copyright 2009 American Chemical Society.

Figure 6: Resonance-enhanced multiphoton ionization setup with a laser ablation source. The two-color variant is shown, where λ_1 and λ_2 are the excitation and ionization lasers, respectively.[87]

Figure 7: Ions are mass-selected by a quadrupole before being injected into a 22-pole trap, where they are cooled to 6–10 K with helium. The cold ions can then be excited and fragmented with laser pulses. The second quadrupole is used to filter the fragments, such that a spectrum can be recorded. Reprinted from Ref. 39, with permission from Elsevier.

Figure 8: The $(1)^1A' \leftarrow X\,^1A'$ electronic transition of protonated pyrene measured by a one-color, two-photon excitation/dissociation technique in an ion trap. The bottom trace was measured at 100 K, and the spectrum is characterized by the presence of several hot bands, which disappear when the ions are cooled to 15 K (top trace). Adapted from Ref. 21, with permission of the AAS.

Figure 9: Laser induced inhibition of complex growth schematic for the N_2^+ system in the presence of helium. Most of the N_2^+ molecules are excited to the $A^2\Pi_u$ electronic state, but 4–5% will undergo complexation through a ternary association reaction. Reprinted from Ref. 44 with permission from Journal of Physical Chemistry Letters. Copyright 2013 American Chemical Society.

Figure 10: The $A\,^2\Pi_u \leftarrow X\,^2\Sigma_g^+$ (2, 0) transition of bare N_2^+ measured with the LIICG method. A decrease in the number of N_2^+—He complexes occurs when N_2^+ is excited to the $A\,^2\Pi_u$ electronic state. The rotational transitions are indicated by their fine structure and nuclear spin components. Reprinted from Ref. 44 with permission from Journal of Physical Chemistry Letters. Copyright 2013 American Chemical Society.

Figure 11: Chain length vs. wavelength for DIB candidates with an odd number of carbon atoms. For C_n^- both the $A - X$ and $B - X$ transitions are shown. The area between the dashed gray lines represents the 4400–9000 Å DIB range.

Figure 12: The origin band of the C_3 laboratory spectrum of the $A\,^1\Pi_u \leftarrow X\,^1\Sigma_g^+$ electronic transition shows excellent agreement with astronomical data observed toward several diffuse clouds.[66] The similarities in both band position and rotational profile confirm that C_3 is present in diffuse interstellar clouds. Reproduced from Ref. 66, with permission of the AAS.

Figure 13: Comparison of experimental and astronomical spectra for the $A\ ^2\Pi_g \square\leftarrow X\ ^2\Pi_u$ transition of NC_4N^+ near 5958 Å is shown on the left. The right panel shows rotational profiles simulated over a temperature range of 3–150 K,[76,88] illustrating the effects on both band shape and wavelength. Adapted from Ref. 76, with permission of the AAS.

Figure 14: Cyclic C_{18} was produced in the laboratory and rotational profiles of the origin band of the lowest electronic transition are shown at 100, 50, and 20 K (top, middle, and bottom traces, respectively) in the left panel. DIB absorptions with similar profiles, but centered at different wavelengths, are shown on the right.[6,89] Reproduced from Ref. 88 with permission from Journal of Physical Chemistry A. Copyright 2013 American Chemical Society.

Figure 15: Comparison of the 5069 Å (middle trace)[84] to rotational profiles of the origin band of the HC_4H^+ $A\ ^2\Pi_g \square\leftarrow X\ ^2\Pi_u$ transition at 30 and 60 K. The top two traces assume equilibrium of the spin-orbit and rotational temperatures, whereas the bottom two traces incorporate magnetic dipole transitions.[85] Adapted from Ref. 85, with permission of the AAS.

Figure 16: An experimental spectrum of the $A\ ^2\Pi_g \leftarrow\square\ X\ ^2\Pi_u$ electronic transition of HC_6H^+ is displayed along with a 25 K predicted profile. The bottom four traces show how the profile would change with different collision partner densities (in cm^{-3}) at 60 K; the broad outline includes a velocity dispersion of 18 km s^{-1}.[38] Adapted from Ref. 38 with permission from The Journal of Physical Chemistry A. Copyright 2013 American Chemical Society

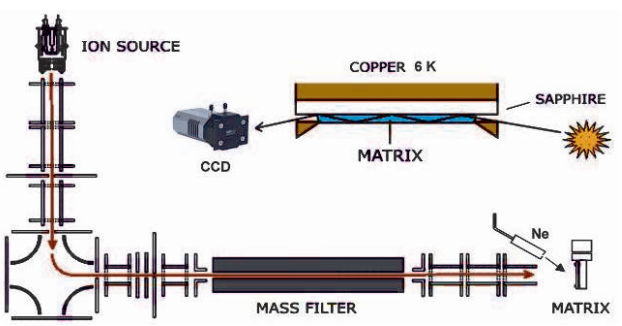
ION SOURCE
COPPER 6 K
SAPPHIRE
CCD
MATRIX
Ne
MASS FILTER
MATRIX

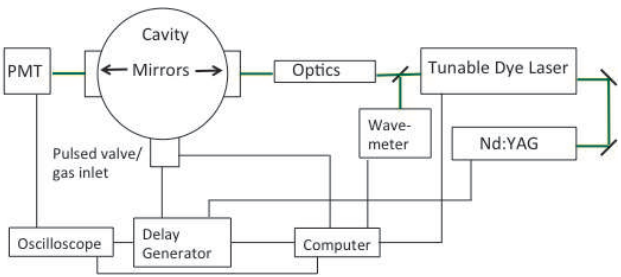
Cavity
PMT
Mirrors
Optics
Tunable Dye Laser
Wave-
meter
Nd:YAG
Pulsed valve/
gas inlet
Oscilloscope
Delay
Generator
Computer

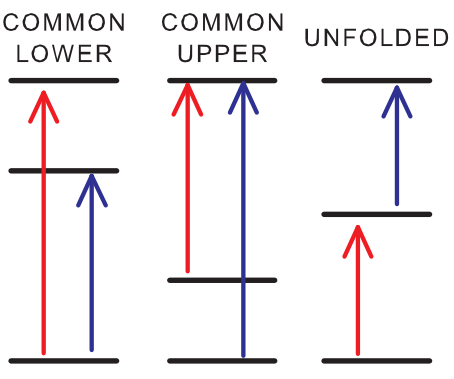
COMMON LOWER
COMMON UPPER
UNFOLDED

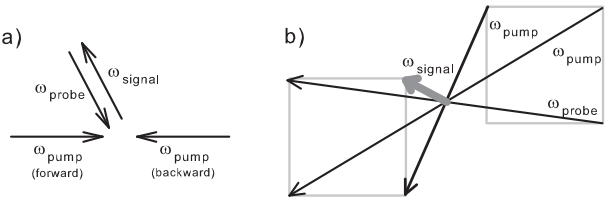
a)
ω signal
ω probe
ω pump
(forward)
ω pump
(backward)
b)
ω pump
ω pump
ω signal
ω probe

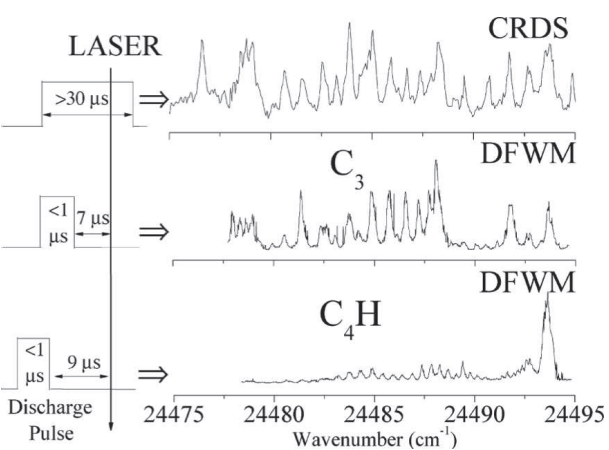
LASER
CRDS
>30 µs
DFWM
C3
<1 µs
7 µs
DFWM
C4H
<1 µs
9 µs
Discharge Pulse
24475
24480
24485
24490
24495
Wavenumber (cm-1)

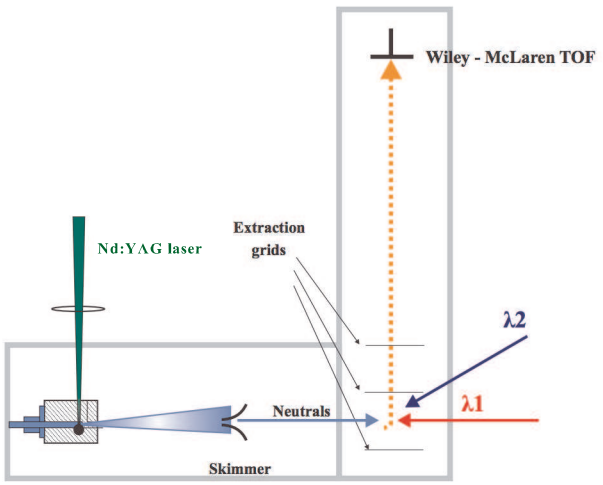
Wiley - McLaren TOF
Nd:YAG laser
Extraction grids
λ2
λ1
Neutrals
Skimmer

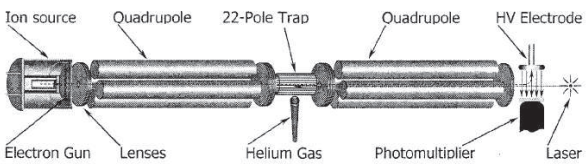
Ion source
Quadrupole
22-Pole Trap
Quadrupole
HV Electrode
Electron Gun
Lenses
Helium Gas
Photomultiplier
Laser

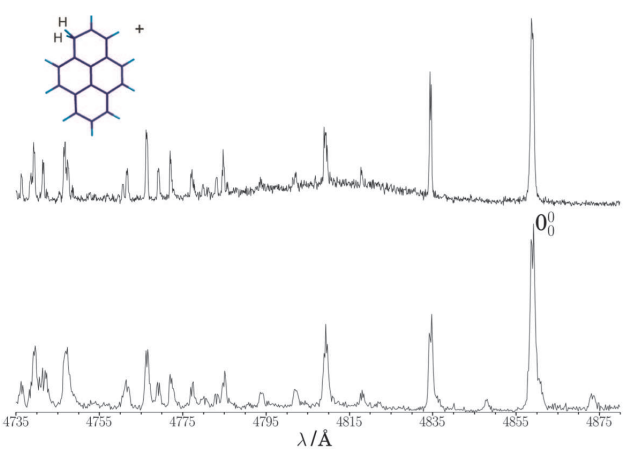
H
H
+
0_0^0
4735
4755
4775
4795
4815
4835
4855
4875
λ / Å

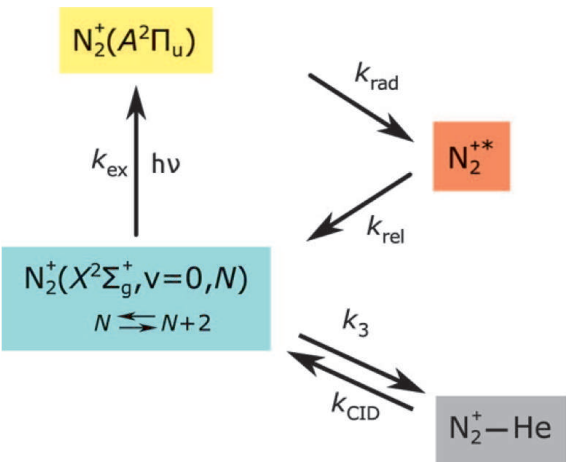
$N_2^+(A^2\Pi_u)$
k_{rad}
k_{ex}
hν
N_2^{+*}
k_{rel}
$N_2^+(X^2\Sigma_g^+, v=0, N)$
$N \rightleftarrows N+2$
k_3
k_{CID}
$N_2^+ - He$

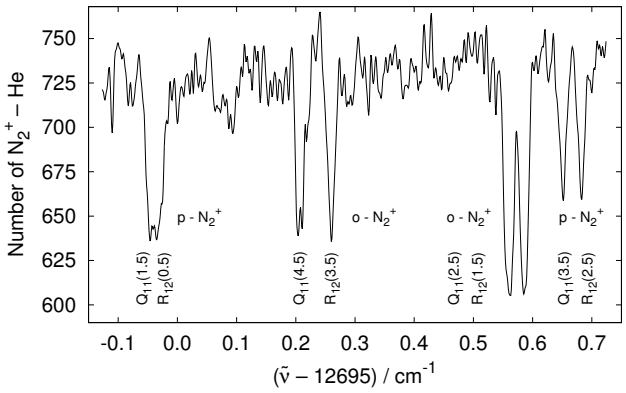
Number of N_2^+ – He
750
725
700
675
650
625
600
-0.1
0.0
0.1
0.2
0.3
0.4
0.5
0.6
0.7
(ṽ – 12695) / cm^{-1}
p - N_2^+
o - N_2^+
o - N_2^+
p - N_2^+
Q_{11}(1.5)
R_{12}(0.5)
Q_{11}(4.5)
R_{12}(3.5)
Q_{11}(2.5)
R_{12}(1.5)
Q_{11}(3.5)
R_{12}(2.5)

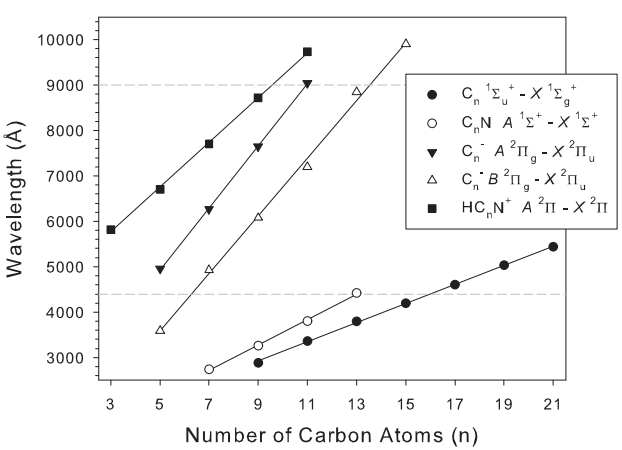
Wavelength (Å)
Number of Carbon Atoms (n)
$C_n\ ^1\Sigma_u^+ - X\ ^1\Sigma_g^+$
$C_nN\ A\ ^1\Sigma^+ - X\ ^1\Sigma^+$
$C_n^-\ A\ ^2\Pi_g - X\ ^2\Pi_u$
$C_n^-\ B\ ^2\Pi_g - X\ ^2\Pi_u$
$HC_nN^+\ A\ ^2\Pi - X\ ^2\Pi$

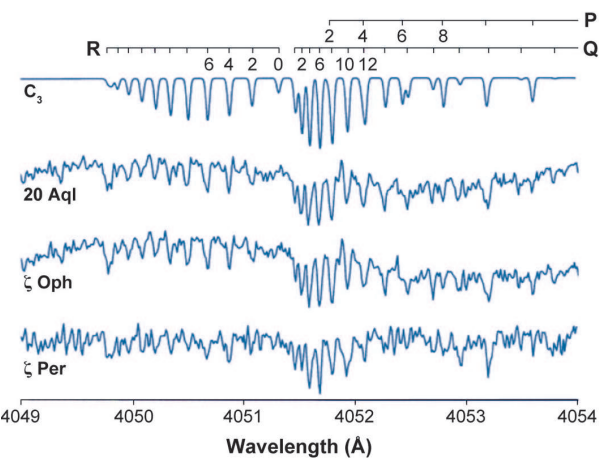
P
2 4 6 8
R
Q
6 4 2 0 2 6 10 12
C3
20 Aql
ζ Oph
ζ Per
4049 4050 4051 4052 4053 4054
Wavelength (Å)

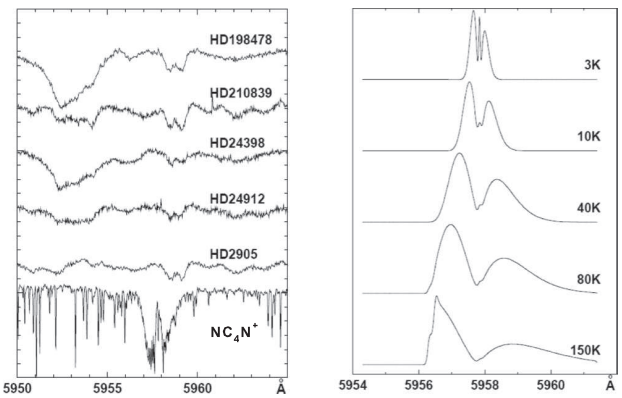
HD198478
HD210839
HD24398
HD24912
HD2905
NC_4N^+
5950
5955
5960
Å
3K
10K
40K
80K
150K
5954
5956
5958
5960
Å

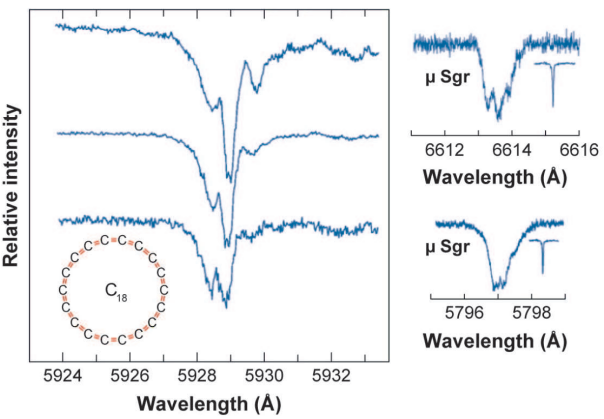
Relative intensity
5924
5926
5928
5930
5932
Wavelength (Å)
C18
μ Sgr
6612
6614
6616
Wavelength (Å)
μ Sgr
5796
5798
Wavelength (Å)

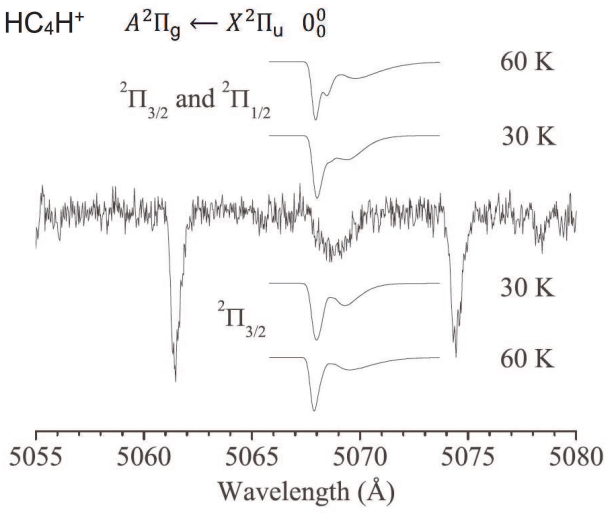
HC4H+ A2Πg ← X2Πu 0₀⁰
60 K
2Π3/2 and 2Π1/2
30 K
30 K
2Π3/2
60 K
5055
5060
5065
5070
5075
5080
Wavelength (Å)

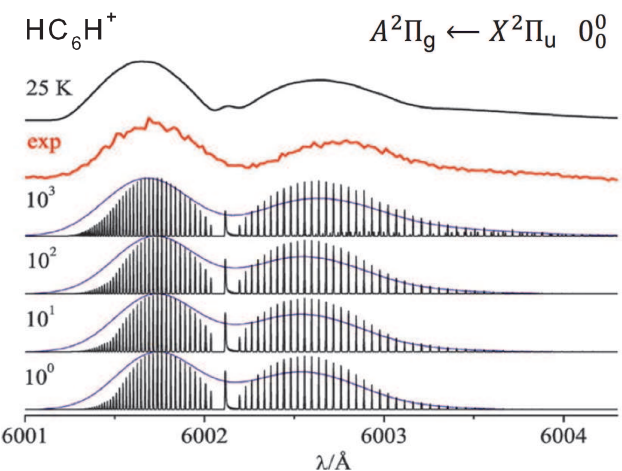
HC6H+
A2Πg ← X2Πu 0 0 0
25 K
exp
10 3
10 2
10 1
10 0
6001
6002
6003
6004
λ/Å

Author Biographies:

John P. Maier received his D. Phil. in physical chemistry from the University of Oxford in 1972, under the supervision of D.W. Turner. Since then, he has been at the University of Basel, first as a postdoctoral fellow and in 1991 was appointed as the physical chemistry department chair. He was elected a Fellow of the Royal Society, London in 1999, and has been awarded several other honors and distinctions. His research interests have focused on the development and use of methods for obtaining electronic spectra of radicals and ions of astrophysical interest.

Lindsay N. Zack received a B.S. in chemistry from Northern Arizona University (2006) and a Ph.D. in physical chemistry from the University of Arizona (2012), under the supervision of L.M. Ziurys. She joined the John P. Maier Group shortly thereafter, where she has worked on cavity ringdown spectroscopy of astrophysically relevant species. Her research interests lie in the areas of high-resolution spectroscopy of metal-bearing molecules and radio astronomy.


NATIONAL
OSIUM ON
RADICALS
PTEMBER 2005
SWITZERLAND
SPEAKERS
CORRESPONDENCE

Textual abstract:

Laboratory spectroscopic methods developed to measure the electronic spectra of astrophysically relevant carbon containing molecules, including radicals and ions, are discussed.